AVALANCHE MODELS FOR SOLAR FLARES
(INVITED REVIEW)

PAUL CHARBONNEAU[1], SCOTT W. McINTOSH[1,2], HAN-LI LIU[1] and THOMAS J. BOGDAN[1]
[1]*High Altitude Observatory, National Center for Atmospheric Research, Boulder, CO 80307-3000, U.S.A.*
[2]*ESA Space Science Department, NASA/GSFC Mailcode 682.3, Greenbelt, MD 20771, U.S.A.*

(Received 7 June 2001; accepted 15 August 2001)

Abstract. This paper is a pedagogical introduction to avalanche models of solar flares, including a comprehensive review of recent modeling efforts and directions. This class of flare model is built on a recent paradigm in statistical physics, known as self-organized criticality. The basic idea is that flares are the result of an 'avalanche' of small-scale magnetic reconnection events cascading through a highly stressed coronal magnetic structure, driven to a critical state by random photospheric motions of its magnetic footpoints. Such models thus provide a natural and convenient computational framework to examine Parker's hypothesis of coronal heating by nanoflares.

1. Introduction

1.1. SOLAR FLARES

Solar flares are the manifestation of a sudden, intense and spatially concentrated release of energy in the corona, causing localized heating up to temperatures of $\sim 10^7$ K, as evidenced by the copious emission of short-wavelength radiation. First observed serendipitously in white light by R. C. Carrington and R. Hodgson in 1859 (see Carrington, 1860)[1], flares have captured the attention of solar physicists ever since. However, it is only recently that space-borne X-ray and extreme ultraviolet (EUV) imaging telescopes have revealed the astonishing range of scales characterizing the flaring phenomenon. The association of most larger flares with magnetic active regions, and their very short onset time, leave little doubt that *magnetic reconnection* is the mechanism responsible for the dynamical release of magnetic energy (see Kulsrud, 1998; Priest and Forbes, 2000; and references therein).

Let $f(E)\,\mathrm{d}E$ be the fraction of flares releasing an amount of energy between E and $E+\mathrm{d}E$ per unit time. A striking statistical feature of the frequency distribution

[1]Hoyt and Schatten (1997, p. 26) mention in passing a report by one Stephen Gray of Canterbury who, on 27 December 1705, saw a 'flash of lightning' near a sunspot; clearly an earlier contender for the first observation of a solar flare.

Solar Physics **203:** 321–353, 2001.

TABLE I

Observational determinations of flare power-law indices for integrated count rate/total energy release (α_E), peak count rate/energy release (α_P), and event duration (α_T). Values taken from (a) Crosby, Aschwanden, and Dennis (1993); (b) Bromund, McTiernan, and Kane (1995); (c) Crosby *et al.* (1998); (d) Shimojo and Shibata (1999); (e) Aschwanden *et al.* (2000a); (f) Shimizu (1995); (g) Krucker and Benz (1998); (h) Parnell and Jupp (2000); (i) Aschwanden *et al.* (2000b).

Data	Instrument	α_E	α_P	α_T	Ref.
HXR	SMM/HXRBS		1.73 ± 0.01	2.17 ± 0.05	a
HXR	ISEE 3/ICE		1.86 ± 0.01	2.40 ± 0.04	b
HXR	WATCH/GRANAT	1.39 ± 0.02	1.59 ± 0.05	1.09 ± 0.03	c
SXR	YOHKOH/SXT		1.7 ± 0.4		d
EUV	TRACE		1.83 ± 0.07		e
HXR	SMM/HXRBS	1.53 ± 0.02	1.67 ± 0.04		a
HXR	ISEE 3/ICE	1.67 ± 0.02	1.92 ± 0.02		b
SXR	YOHKOH/SXT	1.5–1.6			f
EUV	SOHO/EIT	2.3–2.6			g
EUV	TRACE	2.02–2.56			h
EUV	TRACE	1.79 ± 0.08			i

$f(E)$ reconstructed form UV, EUV, and X-ray observations is its power-law form (Drake 1971; Datlowe, Elcan, and Hudson, 1974):

$$f(E) = f_0 E^{-\alpha}, \qquad \alpha > 0\,, \tag{1}$$

which currently holds for eight orders of magnitude in E. Similar power laws are obtained for the peak energy flux (P) and flare duration (T)[2]. Table I offers a compilation, representative rather than exhaustive, of recent determinations of these power-law indices (see also Table I in Crosby, Aschwanden, and Dennis (1993) and Table 1 in Aschwanden, Dennis, and Benz (1998)). The entries have been divided into two groups, the top one relating to power laws involving directly measurable quantities (e.g., peak count rates, total count rate, etc.), and the bottom group to model-dependent determinations (e.g., total energy release in erg).

Converting observed flare X-ray or EUV fluxes to volumetric energy release is a very intricate exercise, involving assumptions regarding the geometrical shape of the flaring region, physical conditions within the flaring volume, and the mechanism responsible for the emission of hard radiation (see, e.g., Lee, Petrosian,

[2]Recall that power-law distributions of the form $f(x) \sim x^{-\alpha}$ do not have a well-behaved average if $\alpha < 2$; the average $\langle x \rangle$ is then always dominated by the largest event measured since $t = 0$, rather than by the accumulating multitude of smaller events. The more one samples the distribution, the larger $\langle x \rangle$ gets!

and McTiernan, 1993; Brown *et al.*, 1998; Mitra-Kraev and Benz, 2001). Furthermore, at finite spatial and temporal resolution, and in the presence of a detection threshold, the observational definition of what constitutes a flare becomes a delicate matter (e.g., Aschwanden *et al.*, 2000a). These observational and data analysis issues account for the significantly different values of the power-law indices reported by different authors, even when working on the same dataset (cf., Table I; see also the discussion in Aschwanden *et al.*, 2000b).

While the mean flaring rate varies by about a factor of twenty in the course of the solar cycle, the power-law indices remain essentially constant (Dennis, 1985; Lu and Hamilton, 1991; Figure 2; Crosby, Aschwanden, and Dennis, 1993, Figure 4). Moreover, distributions constructed for distinct active regions of various sizes show statistically undistinguishable power-law indices (Wheatland, 2000a). Finally, flare-like X-ray emission from stars other than the Sun also appears to be distributed as power laws with similar indices, independent of stellar parameters such as rotation, X-ray luminosity, Rossby number, etc. (see, e.g., Shakhovskaya, 1989; Osten and Brown, 1999; Audard *et al.*, 2000). All this suggests that the flaring *process* is intrinsic to coronal magnetic fields, even though the flaring *rate* may be controlled by extrinsic factors, such as magnetic flux emergence in the photosphere.

1.2. Coronal heating and Parker's conjecture

Ultimately, most of the magnetic energy liberated by the reconnection process ends up heating the plasma surrounding the flaring site. If Equation (1) is taken at face value, the total energy released per unit time by the ensemble of flares is simply

$$E_{\rm tot} = \int_{E_{\rm min}}^{E_{\rm max}} f(E) E \, {\rm d}E = f_0 \left[\frac{E^{2-\alpha}}{2-\alpha} \right]_{E_{\rm min}}^{E_{\rm max}}, \quad \alpha \neq 2 \,, \tag{2}$$

(with $E_{\rm tot} = f_0 \, \log(E_{\rm max}/E_{\rm min})$ for $\alpha = 2$). If $\alpha < 2$ the largest flares dominate the release of energy. Conversely, if $\alpha > 2$ the smallest flares are energetically dominant. On theoretical grounds, E. N. Parker has conjectured that the latter situation holds: that these 'nanoflares' are responsible for coronal heating, and that 'what we see as the X-ray corona is simply the superposition of a very large number of nanoflares' (Parker, 1983, 1988, 1994; see also van Ballegooijen, 1986).

In a nutshell, Parker's idea runs as follows[3]. Stochastic photospheric fluid motions shuffle the footpoints of magnetic coronal loops. The high electrical conductivity of the coronal gas implies that the magnetic field is frozen-in, so that the subsequent dynamical relaxation within the loop results in a complex, tangled magnetic field, essentially force-free everywhere except in numerous small

[3]Parker (1983, Section 1) provides a nice historical review of the development of this idea, starting in the mid-1960s.

electrical current sheets which form spontaneously in highly-stressed regions (see Figure 1.5 in Parker, 1994; for numerical simulations, Mikić, Schnack, and Van Hoven, 1989; Longcope and Sudan, 1994; and Galsgaard and Nordlund, 1996). As the current within these sheets is driven beyond some threshold, reconnection sets in and releases magnetic energy, leading to localized heating[4]. Parker (1988) estimates the energy of a typical nanoflare to be $\simeq 10^{24}$ erg, and argues that they can indeed provide the $\simeq 10^7$ erg cm^{-2} s^{-1} required to heat the corona (Withbroe and Noyes, 1977).

A voluminous body of literature supports the general notion of coronal heating by episodic small-scale energy release events (e.g., Porter *et al.*, 1987; Sturrock *et al.*, 1990; Krucker and Benz, 2000). In the context of Equation (2), Parker's conjecture evidently requires $\alpha > 2$, and observations are now getting close to detecting 10^{24} erg events (Aschwanden *et al.*, 2000b). Current data analyses for total energy release yield a power-law index α_E in the range 1.5–2.6 (cf., Table I), which is too broad a range to confirm or refute Parker's conjecture. Clearly, a theoretical calculation of α_E would be a useful complement to extant observational analyses. *Self-organized criticality* offers an avenue toward this goal.

1.3. SELF-ORGANIZED CRITICALITY

Following the seminal paper of Bak, Tang, and Wiesenfeld (1987, hereafter BTW; see also Bak, Tang, and Wiesenfeld, 1988; Kadanoff *et al.*, 1989), the *sandpile* has become the exemplar of self-organized critical systems[5]. Consider a circular table on which sand grains are dropped one at a time, leading to the buildup of a more or less conical pile. The sandpile steepens until its slope reaches a critical angle (the so-called *angle of repose*) beyond which further addition of sand rapidly leads to *avalanches* sweeping sand down the pile, so that the slope remains close to its critical value[6]. The sandpile is now in a statistically stationary state, with the *average* rate at which sands falls off the table's edge equal to the (constant) rate of sand grain addition. It is a very dynamical stationary state, with relaxation occurring in the form of episodic avalanches involving anywhere from a single grain

[4]Note that in this picture there exist a separation of timescales between energy input to the system (minutes to hours, for photospheric fluid motions on granular scales), and energy release (seconds to minutes, for reconnection and subsequent thermalization under coronal conditions). In other words, the coronal loop is *slowly driven* by footpoint motions, a necessary property of the forthcoming lattice models.

[5]That real piles of sand do not exhibit self-organized criticality (e.g., Nagel, 1992; Jensen, 1998, Section 3.2; Duran, 2000, Chapter 4) in no way diminishes the usefulness of this *gedanken*-sandpile as a pedagogical device, especially since other granular materials do behave in the manner to be described presently.

[6]C.A. Coulomb (of electrostatics fame) suggested in 1773 that the angle of repose (θ_r) could be related to the coefficient of static friction (μ_s) between sand grains as $\mu_s = \tan \theta_r$, a relation that has survived the test of time. For an outstanding introduction to the physics of granular material, see Duran (2000).

to the whole slope. In the language of statistical physics, the correlation length of perturbations extends over the whole system: no matter how big the sandpile, a 'perturbation' (sand grain dropped near the top of the pile) has a finite probability of affecting, through the triggering of a large avalanche, another sand grain located at the bottom of the pile; the system is in a *critical state*.

The critical behavior of the sandpile at the angle of repose is reminiscent of what happens near a thermodynamical phase transition. Yet, here no external controlling parameter (such as temperature) need be finely tuned to achieved criticality; the angle of repose is attained 'naturally' as a consequence of the slow addition of sand grains, and their spatial redistribution by avalanches. The critical state is an *attractor* of the dynamics. It is in that sense that the system is said to be in a state of *self-organized* criticality (hereafter SOC).

A central aspect of SOC systems is that they are interaction-dominated, i.e., their dynamical behavior is an *emergent property* of the relatively simple interaction between many degrees of freedom. It does not matter exactly *how* any two sand grains interact, as long as they do so locally and that their mechanical stability on the slope is subjected to a threshold (e.g., friction between adjacent grains). Such a threshold is in fact crucial, since it allows the existence of multiple metastable states across which avalanches carry the system (for further discussion see Jensen, 1998, Chapter 6; Sornette 2000, Chapter 15).

A universal feature of physical systems in a state of SOC is that they have no preferred scale for the release of 'energy'. In the case of the sandpile, for example, the spectrum $f(n)$ of avalanche size (where n is number of sand grain involved in an avalanche) is expected to be a power law, $f(n) \sim n^{-\alpha}$, with $\alpha \sim 1$. The ubiquitous existence of such power laws, often dubbed '$1/f$' or 'flicker noise', in a wide range of physical systems exhibiting episodic activity (earthquakes and seismic noise emission, landslides and avalanches, cloud formation, magnetospheric substorms, interface growth, and forest fires, to name but a few) has led some authors to offer SOC as the latest 'theory of everything' (see Bak, 1996, for a spirited exposition; also Jensen, 1998; and Turcotte, 1999). Caution is indeed in order here, as power-laws are merely indicative of scale-invariant dynamics, and SOC is but one of many ways to generate scale invariance (see, e.g., Newman and Sneppen, 1996; Sornette, 2000, Chapter 14; in the solar flare context, Rosner and Vaiana, 1978; Litvinenko, 1996; Aschwanden, Dennis, and Benz, 1998; Wheatland and Glukhov, 1998). Nonetheless, it is the observed power-law distribution of flare peak energy that led Lu and Hamilton (1991, hereafter LH91) and Lu *et al.* (1993, hereafter LHMB) to suggest, in these two groundbreaking papers, that the solar coronal magnetic field is in a state of self-organized criticality, and that flares are nothing more than the energy collectively released by an avalanche of small reconnection events.

The remainder of this tutorial/review paper is organized as follows. In Section 2 we introduce a basic lattice model and investigate in detail the properties of the resulting SOC state. In Section 3 we revisit various model ingredients, in the course

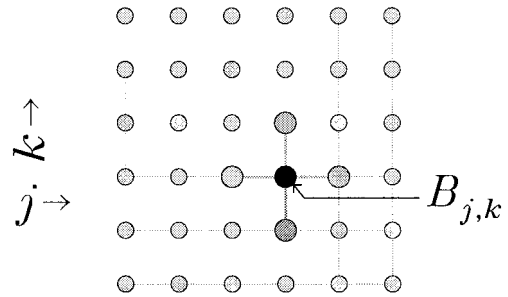

Figure 1. A two-dimensional regular Cartesian lattice. A field quantity B is defined at each node (j, k). Each interior node has four nearest-neighbors (top/down/right/left, in darker gray).

of reviewing the literature on modifications of the Lu and Hamilton model. In section 4 we examine the various possible physical interpretations of the lattice model, and review recent work addressing this important issue. We conclude in Section 5 with a selective overview of what we think are interesting areas for further research in SOC flare models.

2. A Basic Lattice Model

This section is a tutorial introduction to SOC avalanche models of solar flares, using a basic formulation adapted from LHMB.

2.1. THE LATTICE

Avalanche models of the type considered here are defined on a *lattice*, i.e., a network of interconnected *nodes*. Figure 1 shows a simple regular Cartesian lattice with nearest-neighbor connectivity; it has a spatial dimension $D = 2$, linear size $N = 6$, and the total number of nodes is equal to N^D. Consider the node $(j, k) = (4, 3)$, indicated by a black solid dot on Figure 1. This node, like all other interior nodes, has four *nearest-neighbors*. In a D-dimensional generalization of such a lattice, each of the $(N - 2)^D$ interior node has $2D$ nearest-neighbors. We use a vector index $\mathbf{k}$ to label each node of a D-dimensional lattice ($\mathbf{k} \equiv j, k$ for the 2D lattice of Figure 1).

Although spatially discretized, the physical quantity $B_\mathbf{k}$ defined on each lattice node is taken to be a continuous, scalar variable. In the context of solar flares it is common to associate $B_\mathbf{k}$ with some measure of the magnetic field, so that $B_\mathbf{k}^2$ becomes a measure of magnetic energy. The *lattice mean field* ($\langle B \rangle$) and *lattice energy* ($\mathcal{E}_l$) are then

$$\langle B \rangle = \frac{1}{N^D} \sum_\mathbf{k} B_\mathbf{k} \,, \qquad \mathcal{E}_l = \sum_\mathbf{k} B_\mathbf{k}^2 \,, \tag{3}$$

where the sums over **k** stands for D nested sums, each from 1 to N.

2.2. THE STABILITY CRITERION

With B defined on the lattice, each node can be tested for *stability*, as per some specified criterion equivalent to declaring a sand grain unstable if the local slope exceeds the angle of repose. In the original BTW model as well as in a large fraction of subsequent numerical and theoretical work on SOC, a node is deemed unstable if the corresponding value of the field B exceeds some fixed threshold Z_c. Such models are known as 'height-triggered'. In the context of solar flares, most models have followed LH91 in using a criterion based on a measure (ΔB) of the field *curvature*, which for scalar B reads

$$\Delta B = B_{\mathbf{k}} - \frac{1}{2D} \sum_{nn=1}^{2D} B_{nn} , \qquad |\Delta B| > Z_c , \tag{4}$$

where the sum runs over the $2D$ nearest neighbors ('nn') on the Cartesian D-dimensional lattice. While LH91 refer to ΔB as a 'gradient', the left-hand side of Equation (4) has in fact the form of a second-order centered finite difference expression for the D-dimensional Laplacian operator (Galsgaard, 1996). Accordingly, models based on Equation (4) are best referred to as 'curvature-triggered'. While the numerical choice for Z_c has no influence on the general behavior of the model, it must remain non-zero, i.e., *the presence of an instability threshold is crucial*.

2.3. THE REDISTRIBUTION RULE

Once a node is deemed unstable, a procedure is needed to restore stability. This *redistribution rule* is the model's equivalent of having sand grains topple down the sandpile. A natural procedure is to decrease B at the unstable node, and increase it correspondingly at neighboring nodes. Accordingly, we adopt the D-dimensional scalar equivalent of the 3D vector rule introduced in LHMB:

$$B_{\mathbf{k}} \to B_{\mathbf{k}} - \frac{2D}{2D+1} Z_c , \qquad B_{nn} \to B_{nn} + \frac{1}{2D+1} Z_c , \tag{5}$$

with $nn = 1, \ldots, 2D$, and any field redistributed to a boundary node zeroed out (equivalent to letting sand grains fall off the edge of the table). Following the application of Equation (5) one or more of the nearest-neighbor nodes might now exceed the instability threshold, in which case the redistribution rule is to be applied to those nodes, and so on until stability is everywhere restored. The sequence of redistribution events is the model's realization of an avalanche.

The above redistribution rule is *locally conservative* in the lattice variable B, i.e., $B_{\mathbf{k}} + \sum B_{nn}$ remains constant. However, a bit of algebra soon reveals that the lattice energy decreases by an amount

$$e_r = \frac{2D}{2D+1}\left(2\frac{|\Delta B|}{Z_c} - 1\right) Z_c^2 \,. \tag{6}$$

The net energy released by the avalanche at each iteration is thus $\mathcal{E}_r = \sum e_r$, the sum extending over all unstable nodes. If Z_c is just infinitesimally exceeded at a single node, the energy released is

$$e_0 = \frac{2D}{2D+1} Z_c^2 \,. \tag{7}$$

This represents the smallest 'quantum' of energy that can be released by the lattice, and thus makes a convenient energy unit. Redistribution rules other than Equation (5) are of course possible, and it turns out that the character of the SOC state is influenced by this choice. We defer discussion of this important matter to Section 3.

2.4. THE DRIVING MECHANISM

The existence of a globally stationary state requires that the physical quantity defined on the lattice be externally driven. The simplest way to achieve this is to add a succession of perturbations δB at some randomly selected interior nodes. This is the equivalent of dropping sand grains one at a time on the sandpile, and takes place *only* when the lattice is not avalanching. In other words, *driving* occurs much more slowly than *avalanching*, so that a separation of time scales exists between the two mechanisms. Following LH91, we restrict ourselves for the time being to uniform driving, i.e., δB is extracted from a sequence of uniformly distributed random deviates:

$$\delta B \in [\sigma_1, \sigma_2] \,, \qquad \langle \delta B \rangle = \tfrac{1}{2}(\sigma_1 + \sigma_2) \,. \tag{8}$$

The bounds σ_1, σ_2 *must* be chosen so the resulting distribution of perturbation δB has non-zero mean, $\langle \delta B \rangle \neq 0$, so that a net *mean field* grows on the lattice. In addition, for a SOC state to be attained, the driving must be *weak*:

$$|\delta B| / \langle B \rangle \ll 1 \,. \tag{9}$$

For the uniform driver defined by Equation (8), $\langle \delta B \rangle / \langle B \rangle = 10^{-4}$ is a safe upper bound (more on this in Section 3.7)[7]. Here a useful approximate expression for $\langle B \rangle$ is

$$\langle B \rangle \simeq \frac{Z_c}{6D} N^2 \,, \tag{10}$$

[7]LHMB introduced a more stringent condition, namely $|\delta B|/Z_c \ll 1$. This is a necessary condition for SOC in *height-triggered* models, but for curvature-triggered models (cf., Equation (4)) it leads to unnecessarily small δB's, especially on large lattices. Equation (9) is also in better conceptual agreement with Parker's tangled field picture, since the mean increment $\langle \delta B \rangle$ is a fixed fraction of the mean field for any lattice; in the initial, kinematic stage of braiding magnetic fieldlines around one another, the tangential component induced by footpoint motions is expected to be proportional to the mean (vertical) magnetic field (see Parker, 1988, Section 5).

which is accurate to a few percent for $D = 2, 3$ (and exact for $D = 1$). The number of iterations needed to reach SOC from a $B_{\mathbf{k}} = 0$ initial condition is then $\sim N^D \times \langle B \rangle / \langle \delta B \rangle$, which can get quite high for large N and D since $|\delta B|/\langle B \rangle \ll 1$ is required[8].

2.5. ALGORITHMIC IMPLEMENTATION

We have now defined all the ingredients required to set up a simple simulation. A minimal pseudo-code for such a simulation is shown on Figure 2. It consists of a time-like iteration ($i := 1, N_i$) involving: (1) a loop over all interior nodes, checking for local stability; (2) a second lattice loop updating the $B_{\mathbf{k}}$'s; and (3) addition of a field increment at some randomly selected lattice node $\mathbf{k}^*$, taking place only if all nodes are found to be stable at the current iteration.

Note how in the first lattice loop a stability check is first made at each interior node ($\mathbf{k} := 2, N - 1$), and if instability is detected the increments/decrements in B associated with the redistribution rule defined by Equation (5) are *accumulated* in the D-dimensional work array C. Only after this first sweep over the lattice is completed is the field synchronously updated at all interior nodes. Applying the redistribution rules immediately upon detecting an unstable node would introduce a spatial bias in the avalanching process, according to the manner in which the lattice sweep is carried out, clearly an undesirable break of isotropy.

2.6. REACHING THE SOC STATE

All we need now is a good random number generator (get one, e.g., in Press *et al.*, 1992, Chapter 7), and we are ready to compute. Figure 3 shows the time series of energy release (panel A) and lattice energy (panel B) resulting from running an algorithm similar[9] to that listed on Figure 2 on a $N^D = 48^2$ lattice for $N_i = 1.6 \times 10^7$ iterations, with model parameters $Z_c = 5$, $\sigma_1 = -0.2$, $\sigma_2 = 0.8$, and initial condition $B_{\mathbf{k}} = 0$. As B grows on the lattice under the influence of driving (see inset B1), equivalent to the buildup of the sandpile, avalanches start to occur. Their peak size increases gradually as the mean field and lattice energy grow. After about 13 million iterations, the lattice energy abruptly levels off, a transition accompanied by an equally sudden increase in the size of the largest avalanches, which now begin to span the whole lattice. This is the much-awaited SOC state.

As can be seen on inset A1, avalanches are discrete events, well separated in time and showing considerable temporal structure. From the point of view of the mean-field (inset B1), the avalanches look like very low amplitude 'ripples'

[8]For fixed Z_c, σ_1, σ_2, as in LHMB, the scaling is even worse: $\sim N^{2D}$.

[9]While mathematically correct and didactically preferable, the algorithm listed on Figure 2 is inefficient in a number of ways, most notably by checking stability at every interior node at each iteration, even if the previous iteration only saw the addition of a field perturbation at a single random node $\mathbf{k}^*$!

```
B_k := 0,        k = 1, N                    initial condition
C_k := 0,        k = 1, N                    work array
s := 2D + 1                                  a convenient constant
for i := 1, N_i do                           time-like iteration loop
    e := 0
    for k := 2, N − 1 do                     first lattice loop
        Z_k := B_k − (1/2D) Σ B_nn           compute curvature
        if |Z_k| > Z_c then                  node is unstable
            C_k := C_k − (2D/s) Z_c          accumulate redistributions
            C_nn := C_nn + (1/s) Z_c         (eqs. (5))
            g := (2D/s)(2|Z_k|/Z_c − 1) Z_c^2   nodal energy release, eq. (6)
            e := e + g                       accumulate energy release
        endif
    endfor
    if e > 0 then                            an avalanche occurred
        for k := 2, N − 1 do                 update lattice
            B_k := B_k + C_k                 update field array
            C_k := 0                         zero work array
        endfor
    else                                     no avalanche: drive field
        k* :=irandom(D, N)                   pick random interior node
        δB :=random(σ_1, σ_2)                random increment, eq. (8)
        B_k* := B_k* + δB                    update field at node
    endif
endfor
```

Figure 2. Minimal pseudo-code for the SOC lattice model described in the text. The outermost loop is the time-like iteration, D is the lattice dimension, N the linear lattice size, and $\mathbf{k}$ is a D-dimensional integer array that uniquely labels each lattice node. The work array C is used to accumulate the field increments/decrements associated with the application of the redistribution rule to unstable nodes. Note that the lattice loops span only interior nodes, so that $B_{\mathbf{k}} = 0$ remains enforced at all boundary nodes. The function `irandom` returns a D-dimensional integer array $\mathbf{k}^*$ with each element randomly selected from 2 to $N - 1$, thus identifying a randomly selected interior node. The function `random` returns a number extracted from a sequence of random deviates uniformly distributed in the interval $[\sigma_1, \sigma_2]$.

propagating along the mean field, reflecting the fact that avalanches release only a very small fraction of the lattice energy (cf., Figure 3(B) and inset B2).

2.7. Properties of the SOC state

The SOC state is stationary in the sense that over long timescales, $\langle B \rangle$ and $\mathcal{E}_l$ neither grow nor decay. However, the way in which this happens is somewhat peculiar. While the average driving rate is constant, energy dissipation occurs in a bursty, intermittent manner, via avalanches that are self-similar in space and time,

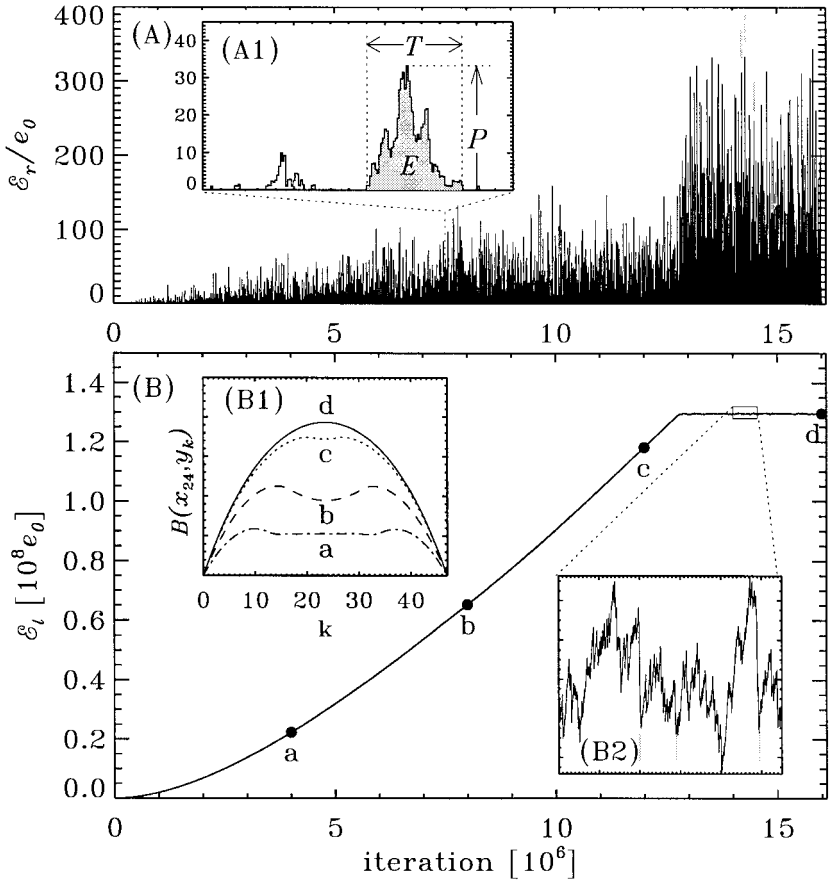

Figure 3. Time series of energy released in avalanches (A) and lattice energy (B). The underlying model is defined on a $N^D = 48^2$ lattice, with initial condition $B_{\mathbf{k}} = 0$ and all energies expressed in units of the minimal single-site energy release e_0 (Equation (7)). The inset A1 shows a small portion of the energy release time series, and illustrates the fundamentally discrete nature of the energy release process, occurring in bursts of all sizes, well separated in time. The peak energy release P, total energy E and duration T are readily extracted from such time series. The inset B1 shows four 1D B-cuts along the middle of the lattice, extracted at epochs indicated by the solid dots on the lattice energy curve on (B), and illustrates the growth of the 'mean-field' towards SOC. Inset B2 is a closeup on the lattice energy curve, showing how sharp drops (gray vertical line segments) correspond to peaks in the energy release time series on (A) (also flagged by gray line segments). The SOC state sets in at the point where the lattice energy levels off to a stationary value. Note on (A) how the peak energy release (i.e., the size of avalanches) increases abruptly once the SOC state is reached.

i.e., they have no characteristic spatial or temporal scale[10]. It is important to realize that large avalanches are *essential* to the existence of the SOC state. Because the redistribution rule is conservative in B, and the driving is such that $\langle \delta B \rangle \neq 0$, stationarity can only be maintained if B is zeroed out at the boundaries at the same average rate at which it is added by the driving process. The required transport of B to the boundaries is mostly accomplished by large avalanches. In other words, large avalanches set up the long-range spatial correlations that are responsible for establishing the proper balance between B-conservative internal avalanches that only redistribute B, and B-dissipative avalanches reaching the lattice boundaries. This delicate balance is central to the SOC state (for further discussion, see Sornette, 2000, Chapter 15).

The solid-line histogram on Figure 4 is the frequency distribution of the curvature measure, ΔB (see Equation (4)), normalized to its instability threshold Z_c. The distribution is constructed from a non-avalanching iteration snapshot of a $N^D = 128^2$ lattice again with $Z_c = 5$, and excluding boundary nodes. Statistically undistinguishable distributions are obtained for other lattice sizes, or other values of Z_c. The ΔB distribution is sharply peaked, with a mean at $\Delta B / Z_c \simeq 0.59$. This corresponds to the overall curvature of the mean-field set up across the lattice in the SOC state (see solid line on B1 inset of Figure 3). In curvature-triggered models, it is thus essential to pin down the field at the boundaries (see Galsgaard, 1996, for more on boundary conditions), and to have a driving mechanism with a non-zero mean. Interestingly, ΔB distributions for 3D models (dotted histogram on Figure 4) have the same mean and similar overall shape, though they are statistically distinct from the 2D distributions. Driving slowly pushes the distribution to the right, but avalanches counteract this tendency by pushing it back to the left.

2.8. Characterization of avalanches

We now turn to the avalanches themselves, for which we define five quantities to characterize temporal and spatial behavior. The peak energy release (P) is the maximum energy released in a single iteration in the course of an avalanche. The duration (T), is the number of iterations from the onset of the avalanche to the recovery of stability across the whole lattice. The total energy E is the sum of all energy released at all avalanching nodes in the course of the whole avalanche, i.e., the gray area under the energy release curve on inset A1 of Figure 3. The remaining two measures refer to the geometrical properties of the avalanches. Figure 5 shows a sequence of three snapshots of an ongoing avalanche, computed on a $N^D = 128^2$ lattice (see also the animation on the CD accompanying this Journal issue). The area (A, see Figure 5) is the set of all lattice nodes having gone unstable at least

[10]More precisely, functional relationships such as power-laws are *self-similar*, in that they remains invariant under a change of scale in either variable. For example, introduce the scaling $E' = aE$ in Equation (1). It is easily verified that the rescaling $f' \to a^\alpha f$ recovers $f' = f_0 E^{-\alpha}$. *Fractals* are the geometrical expression of self-similarity.

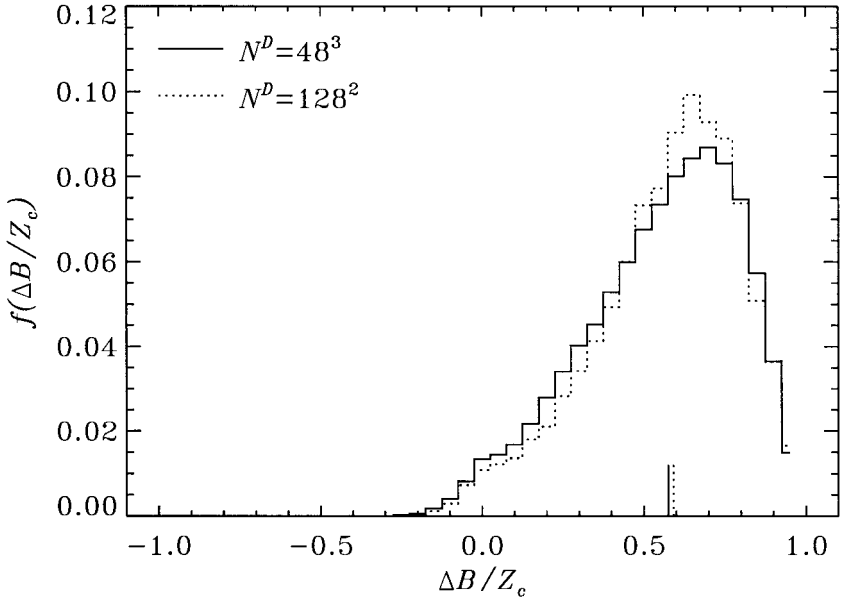

Figure 4. Distribution of local curvature ΔB (normalized to the critical threshold Z_c) for various lattices. The distributions are constructed from a non-avalanching iteration in the SOC state. The vertical line segments are the means $\langle \Delta B/Z_c \rangle$.

once in the course of the avalanche. The resulting cluster of nodes is the vaguely Switzerland-like white shape on Figure 5(D). A useful estimate of its characteristic linear size R is given by its radius of gyration:

$$R^2 = \frac{1}{M} \sum_{i=1}^{M} |\mathbf{r}_i - \mathbf{R}_0|^2 \ , \tag{11}$$

where the sum runs over the M nodes that are part of the cluster, and $\mathbf{R}_0 = (1/M) \sum \mathbf{r}_i$ is the cluster's center of mass. Physically, R is simply the radius of the thin spherical shell (circular ring in 2D) having the same 'mass' and moment of inertia as the original cluster (see Stauffer and Aharony, 1994, Section 3.2).

These five quantities are related via well-defined, albeit statistical power-law relationships of the general form $\log(y) \sim \gamma_{xy} \log(x)$, where x, y stand for any two of the five measures defined above (see LHMB, Figure 7)[11]. Figures 6(A) and 6(B) illustrates two such power-law correlations for which observational counterparts are available (Crosby, Aschwanden, and Dennis, 1993; Bromund, McTiernan, and Kane, 1995). The exponent γ_{RA} is the *fractal dimension* of the avalanche. The time-integrated avalanche area (Figure 5(D)) is a compact object, so that $\gamma_{RA} = D$ to a percent or better. If however one uses the spatial distribution of unstable nodes

[11] Since they define power laws, the γ's are related to one another via relationships of the form $\gamma_{zx} = \gamma_{zy} \times \gamma_{yx}$; also, $\gamma_{yx} = 1/\gamma_{xy}$, and, in terms of the α-indices soon to be introduced (Equation (12) below), $\gamma_{xy} = (\alpha_x - 1)/(\alpha_y - 1)$.

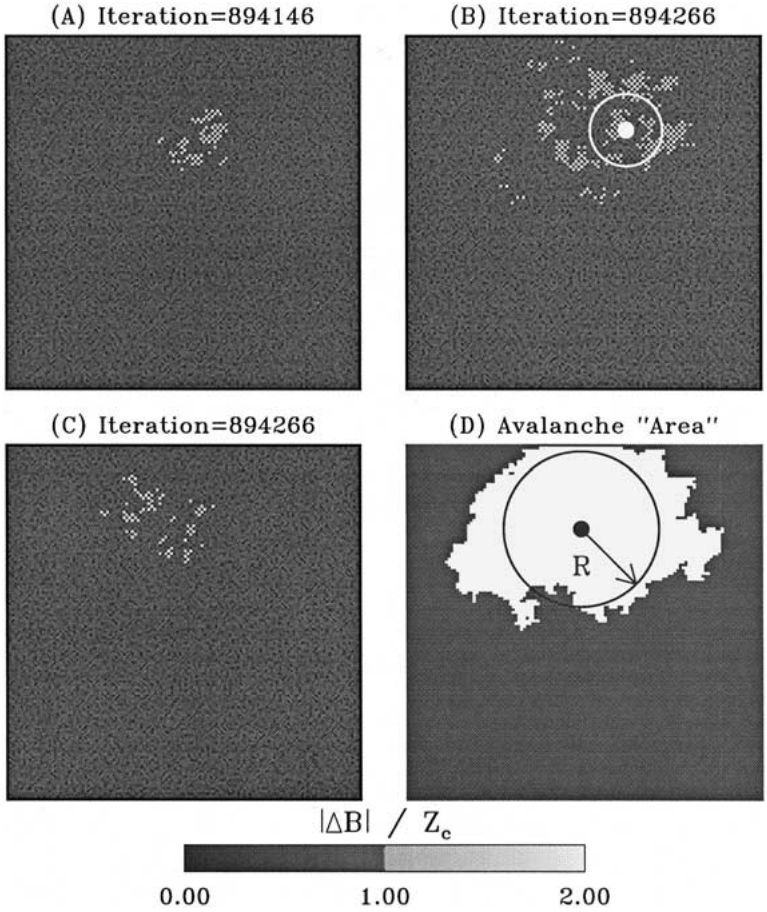

Figure 5. Snapshots of an ongoing avalanche on a $N^D = 128^2$ lattice (A–C). (B) is extracted at the peak of the avalanche. The gray scale encodes ΔB, with the bright checkerboard-patterned regions corresponding to unstable nodes. Note how spatially fragmented the avalanche becomes once it gets underway. The white cluster on (D) shows the total area of the avalanche.

at the avalanche peak (Figure 5(B)) to define A and R, then $\gamma_{RA}(P) < D$ (see Table II further below).

2.9. Statistics of avalanches

Armed with the above definitions for E, P, T, A, and R, we can run the lattice models over a great many iterations, collect avalanche data, and build frequency distributions for these quantities. Figure 6(C–E) shows the results of this exercise for E, P and T (histograms), for a 10^7 iteration run on a $N^D = 32^3$ lattice, in the course of which $\simeq 2.5 \times 10^6$ avalanches were recorded. All quantities exhibit well-defined power laws spanning many orders of magnitude. The solid lines on Figure 6(A–C) are nonlinear least-squares fits of the general form

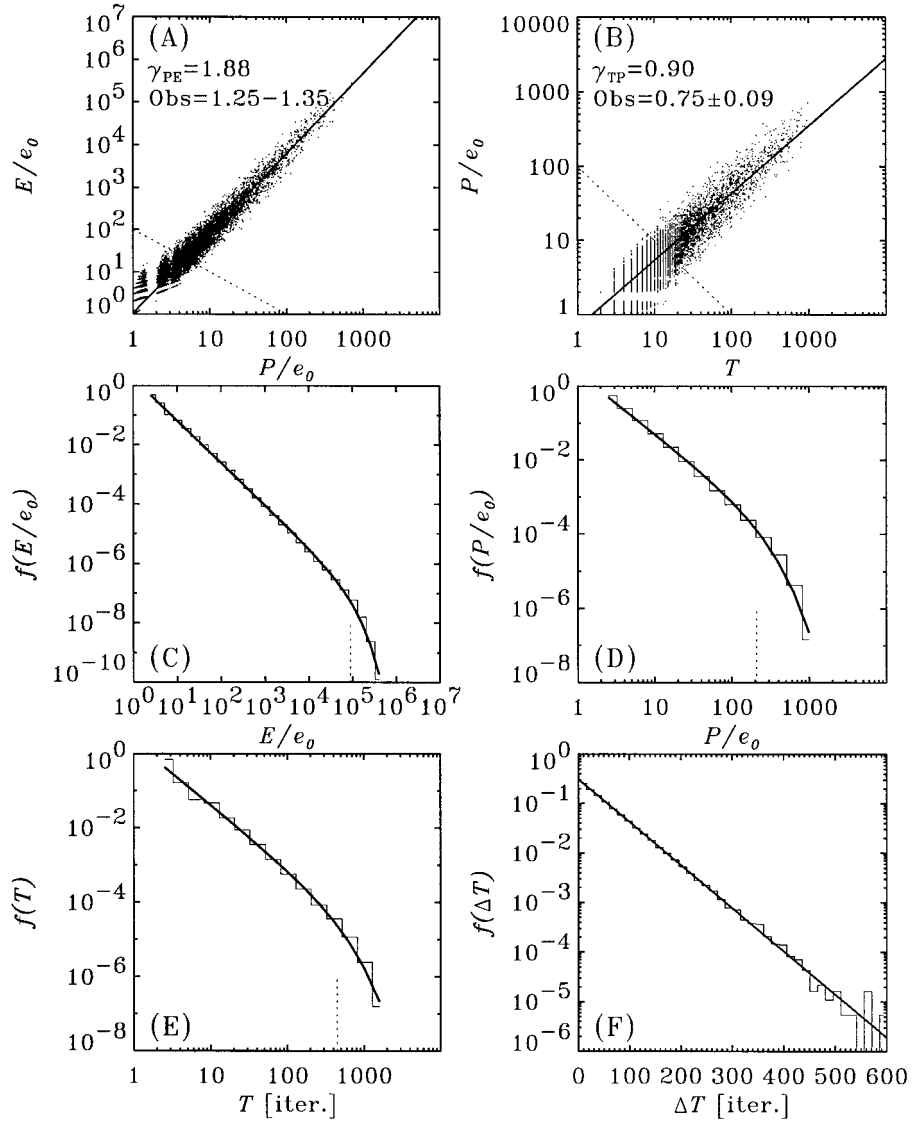

Figure 6. Statistical properties of avalanches in a representative 10^7 iteration run carried out on a $N^D = 32^3$ lattice. (A) and (B) show the typical power law cross-correlation between avalanche parameters, with power-law least-squares fits carried out using only data above the diagonal *dotted line*, because of clustering of small avalanche parameters due to the discrete nature of the lattice. Observationally inferred indices are also listed. (C–E) are normalized frequency distributions for E, P, T, with least-square fits (*solid lines*) to Equation (12). The *vertical line segments* correspond to the length scale x_c of the cutoff function $G(x, x_c)$. (F) shows the frequency distribution of waiting times ΔT, which is very well fit by an exponential distribution.

TABLE II

Power-law indices for total energy (E), peak energy (P), and duration (T) of avalanches in various lattice models, obtained by least-squares fits of Equation (12) to frequency distributions such as plotted on Figure 6. The fractal dimension $\gamma_{RA}(P)$ of the cluster of avalanching nodes at the peak of avalanches (as on Figure 5(B)) is also listed. The leftmost columns gives the length n (in units of 10^7 iterations) of the sets of 10 independent time series used to build the avalanche statistics for each lattice (see text).

N^D	α_E	α_P	α_T	$\gamma_{RA}(P)$	n
32^2	1.429 ± 0.001	1.741 ± 0.005	1.711 ± 0.002	1.610 ± 0.022	0.5
64^2	1.417 ± 0.002	1.725 ± 0.007	1.715 ± 0.003	1.600 ± 0.020	1.0
128^2	1.402 ± 0.002	1.704 ± 0.004	1.697 ± 0.002	1.572 ± 0.032	1.0
256^2	1.408 ± 0.001	1.692 ± 0.005	1.700 ± 0.004	1.552 ± 0.021	1.5
512^2	1.416 ± 0.005	1.707 ± 0.005	1.721 ± 0.007	1.561 ± 0.042	2.0
1024^2	1.421 ± 0.004	1.731 ± 0.005	1.723 ± 0.008	1.581 ± 0.038	2.0
16^3	1.451 ± 0.003	1.855 ± 0.008	1.650 ± 0.009	1.779 ± 0.025	1.0
24^3	1.464 ± 0.003	1.875 ± 0.007	1.705 ± 0.003	1.768 ± 0.034	1.0
32^3	1.464 ± 0.003	1.890 ± 0.006	1.737 ± 0.006	1.799 ± 0.028	1.0
48^3	1.487 ± 0.007	1.915 ± 0.009	1.793 ± 0.008	1.782 ± 0.023	1.5
64^3	1.491 ± 0.006	1.923 ± 0.007	1.787 ± 0.007	1.793 ± 0.031	2.0
128^3	1.485 ± 0.004	1.916 ± 0.008	1.788 ± 0.005	1.777 ± 0.022	2.0

$$f(x) = f_0 x^{-\alpha_x} G(x; x_c) \,, \tag{12}$$

where as before x stands for E, P, etc, and $G(x; x_c)$ is a cutoff function characterized by a length scale which is expected to scale with grid size as yet another power law, $x_c \sim N^\beta$, implying *finite-size scaling* (Kadanoff *et al.*, 1989). LHMB used an exponential cutoff function $\exp(-x/x_c)$ and demonstrated finite-size scaling (see their Figure 3)[12]. The fits (solid lines on Figure 6(C–E)) are carried out on $\log(f)$ and for logarithmically constant bin width $\Delta \log x = 0.2$, each bin being assigned a weight $\sqrt{N}$, under the assumption of Poisson statistics. The first 2 bins are omitted from the fits, because of the discrete nature of the grid distorts the frequency distributions for the smaller avalanches.

The best-fit indices for a variety of lattice sizes and dimensions are listed in the top section of Table II. These values are in good agreements with the results listed in Table 1 of LHMB and Table II of Edney, Robinson, and Chisholm (1998), the slight remaining differences being due – we strongly suspect – to the different

[12]The existence of finite size scaling is considered to be a *sine qua non* condition for a system to be deemed *critical*. Systems sharing the same set of α and β indices are said to belong to the same *universality class*. Here a logistic function gives a better fit to the cutoff, but this matters little in the determination of the α-indices, except on small lattices.

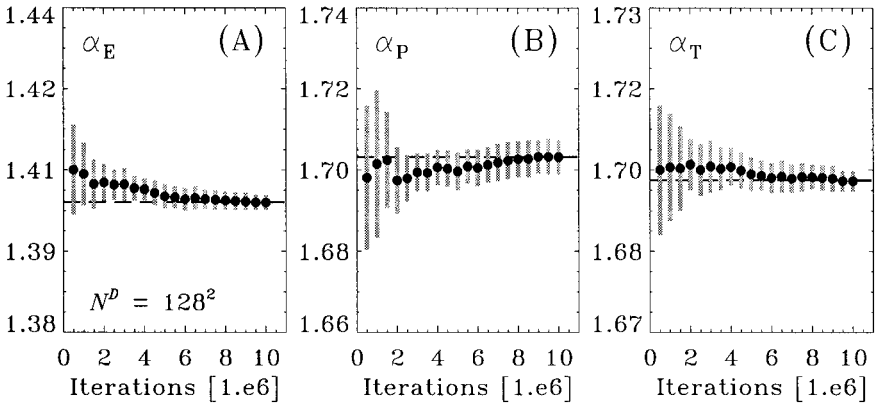

Figure 7. Variations of the least-squares fit power-law indices α_E, α_P and α_T as a function of the length of the time series used to construct the frequency distributions. The *solid dots* are the mean of ten independent $N^D = 128^2$ runs, with the *gray vertical bars* spanning the 1σ r.m.s. deviation about the mean. The *dashed horizontal lines* are included as a guide to the eye, and correspond to the mean of the three rightmost data points.

manners each group went about carrying out the fits. Note how (1) the indices converge reasonably rapidly as lattice size is increased; (2) they do not differ greatly between 2D and 3D lattices; (3) for either $D = 2$ or 3, the α-indices fall nicely within the ranges set by observational inferences (cf., Table I), with the worst discrepancy occurring for α_T, which turns out to be the hardest to infer reliably from observations. Our basic model is doing pretty well at reproducing flare statistics!

It is important to note that the long-range (spatial and temporal) correlations characterizing the SOC state can lead to significantly different power law indices if the runs are not carried out over sufficiently many iterations. This is illustrated on Figure 7, for a sequence of $N^D = 128^2$ runs. The power law indices are calculated for the first 5×10^5 iterations, 10^6 iterations, 1.5×10^6, and so on up to the full length of the run, here 10^7 iterations. This procedure is repeated for 10 independent such runs, and the average power law indices are then calculated and plotted (solid dots) as a function of run length, together with the $\pm\, 1\,\sigma$ r.m.s. deviation about the corresponding mean values. The index values and error estimates listed in Table II were computed in this manner. The larger the lattice, the longer the simulation must be run to recover stable α-indices. Here for $N^D = 128^2$, a few 10^6 iterations are needed for the values of the indices to stabilize to within $\pm$ 0.01, exemplifying the natural variability of the SOC state.

2.10. THE WAITING TIME DISTRIBUTION

Another interesting quantity is the waiting time (ΔT), defined as the number of iterations between the end of an avalanche to the onset of the next. These show no correlation with the size of the next avalanche (LHMB, Figure 6; Georgoulis,

Vilmer, and Crosby, 2001, Section 4.3), and neither do solar flares (e.g., Crosby, Lund, and Sunyaev, 1998; Wheatland, 1999). This is contrary to the predictions of stochastically triggered energy loading models, such as those originally proposed by Rosner and Vaiana (1978; see Lu, 1995c; but also Wheatland and Glukhov, 1998). Essentially, avalanche models lack such a correlation because the avalanches only release a small fraction of the energy stored in the lattice, so that two large flares can occur closely spaced in time, without the need for an energy 'reloading' interlude.

The waiting times distribution (WTD) is plotted on Figure 6(F), and is very well fit by an exponential $f(\Delta t) = \lambda_0^{-1} \exp(-\lambda_0 \Delta t)$, where λ_0 is the mean flaring rate over the complete time series (number of avalanches over number of non-avalanching iterations); this behavior indicates that the triggering mechanism is a Poisson process, which is precisely what one would expect from the uniform driver of Section 2.4 (see Wheatland, Sturrock, and McTiernan, 1998). It also stands in marked contrast to observational inferences of the WTD, which are characterized by a power law tail at large waiting times (Boffeta *et al.*, 1999; Wheatland, 2000b; Lepreti, Carbone, and Veltri, 2001). This apparent failure of our basic model will be readily corrected in Section 3 below.

2.11. Initialization formula

We end this tutorial section with a useful practical tip. In the SOC state, all memory of the initial condition is lost; since it is the properties of the SOC state that are usually of interest, initializing the lattice with $B_{\mathbf{k}} = 0$ is far from optimal, in view of the subsequent lengthy driving to SOC (at best $\sim N^D$, as per Section 2.4). A more efficient initialization procedure can be designed upon recalling that the stability criterion given by Equation (4) has the form of a second-order centered finite difference representation of the D-dimensional Poisson equation:

$$\nabla^2 B(\mathbf{x}) = -\frac{2DZ_c}{N^2}\,, \qquad 1 \le \mathbf{x} \le N\,, \tag{13}$$

A general D-dimensional solution to $\nabla^2 B = 1$ on the unit hyper-cube with boundary condition $B = 0$ is

$$B(x_1, x_2, \ldots, x_D) = \frac{1}{2} x_1 (x_1 - 1) + (1 - \delta_{1,D}) \frac{4}{\pi^2} \sum_{n_1=0}^{\infty} \left\{ \frac{\sin(\pi(2n_1+1)x_1)}{(2n_1+1)^3} \times \right.$$
$$\left. \times \left[\prod_{k=2}^{D-1} \left(\frac{4}{\pi} \sum_{n_k=0}^{\infty} \frac{\sin(\pi(2n_k+1)x_k)}{(2n_k+1)} \right) \right] \frac{\cosh(\pi\Delta(2x_D - 1))}{\cosh(\pi\Delta)} \right\}\,, \tag{14}$$

where

$$\Delta^2 = (n_1 + \tfrac{1}{2})^2 + (n_2 + \tfrac{1}{2})^2 + \cdots + (n_{D-1} + \tfrac{1}{2})^2\,, \tag{15}$$

and $\delta_{1,D}$ is the Kronecker delta. An exact solution to Equation (13) is then readily constructed. Upon initializing the simulation with such a solution, SOC is rapidly

attained[13], following an initial avalanching phase occurring primarily because the ΔB distribution is not a δ-function in the SOC state (see Figure 4).

3. Variations on a Theme

Evidently, many variations on the original LH91/LHMB model can be constructed. The past decade has witnessed the publication of many such variations and elaborations, to a review of which we now turn.

3.1. Scalar versus vector fields

LH91 and LHMB originally formulated their model in terms of a 3D vector field $\mathbf{B_k}$ defined at each lattice node, each component being independently driven as described in Section 2.4. This leads to a mean-field configuration having $B_x = B_y = B_z$ everywhere, thus requiring a single degree of freedom per node, e.g., $|\mathbf{B}|$, to describe the 3D vector field (Robinson, 1994), which brings us back to the basic model of Section 2. The numerical study carried out by Edney, Robinson, and Chisholm (1998) has shown that for a given D, the vector and scalar versions of this model belong to the same universality class. With a few exceptions, most subsequent models have adopted the less computationally demanding scalar version.

3.2. Stability criteria and redistribution rules

Experience with the height-triggered BTW model suggests that variations on the instability criterion and redistribution rule are the alterations most likely to change the character of the SOC state. This is found to carry over to the curvature-triggered model.

Zirker and Cleveland (1993) have studied a $N^D = 32^2$ model involving the *eight* nearest neighbors to define the stability criterion. In addition, their redistribution rule is both stochastic and anisotropic: if node $\mathbf{k}$ is deemed unstable, they redistribute half of $B_\mathbf{k}$ to only two randomly selected neighbors. The slowly-driven version of their Model A yields $\alpha_E = 1.45$, similar to the basic model of Section 2. This suggests that both versions of the model belong to the same universality class, as appears to be the case within the original height-triggered modeling framework of BTW (Chessa *et al.*, 1999).

L. Vlahos and collaborators have studied a variety of $D = 3$ models incorporating anisotropic stability thresholds and redistribution rules (see Vlahos *et al.*,

[13] In practice it is optimal to initialize the simulation with the solution B^* scaled down by a numerical factor f corresponding to the mean of the ΔB distribution appropriate to the lattice under study ($f = 0.59$ for $D = 2$ or 3 on a regular Cartesian lattice, see Figure 4). We reiterate that careful monitoring of the lattice energy is still here the safest way to ascertain whether or not the SOC has been reached.

1995; Georgoulis and Vlahos, 1996, 1998). In Vlahos *et al.* (1995)'s Model B, the usual stability criterion (Equation (4)) is replaced by *six* independent criteria, one per nearest neighbor:

$$\Delta B_{nn} = B_{\mathbf{k}} - B_{nn} \ , \qquad |\Delta B_{nn}| > Z_c \ , \qquad nn = 1, \ldots , 6 \ . \tag{16}$$

Redistribution only occurs with the n^* (≤ 6) nearest neighbor nodes for which the stability criterion is exceeded:

$$B_{\mathbf{k}} \rightarrow B_{\mathbf{k}} - \frac{6}{7} Z_c \ , \qquad B_{nn} \rightarrow B_{nn} + \frac{1}{n^*} \frac{6}{7} Z_c \ , \qquad nn = 1, \ldots , n^* \tag{17}$$

(compare to Equation (5)). Because stability is more easily violated with the stability criterion given by Equation (16), and fewer nodes take part in the redistribution, the model favors smaller avalanches, and consequently, avalanche size-distributions are characterized by steeper power laws than in the basic isotropic model of Section 2. Vlahos *et al.* (1995) report $\alpha_E \simeq 3.5$, $\alpha_P \simeq 3.6$, and α_T in the range 7–11 over a wide range of lattice sizes.

Vlahos *et al.* also experimented with two models where a redistribution event lowers the stability threshold Z_c of its nearest-neighbor nodes, by an amount proportional to the local field gradient ΔB_{nn} at the time of instability. This was found to have very little effect on the resulting power-law indices. LHMB and MacKinnon and Macpherson (1997) also reported introducing random spatial fluctuations in Z_c, without significant changes on the frequency distributions.

Georgoulis and Vlahos (1996, 1998) have presented results for a hybrid model where the above stability criterion and redistribution rule are used concurrently with the standard isotropic criterion and redistribution rules of Section 2.2 and 2.3. In this case the frequency distribution of avalanche parameters are characterized by a double power law (see Figure 1 in Georgoulis and Vlahos, 1998). The steeper power law is confined to small events, and has indices similar to Model B of Vlahos *et al.* (1995), while the power laws for larger events are comparable to those of the standard isotropic model.

MacKinnon and Macpherson (1997) have considered a variation on the basic model which includes *non-local* effects. Whenever a node becomes unstable, the usual redistribution rule is applied; in addition, the Z_c value at one or more randomly selected nodes elsewhere in the lattice is halved at the next iteration. This can 'spontaneously' trigger a secondary avalanche. Having more than two non-local nodes thus perturbed per redistribution event is found to induce significant departures from the original power-laws, and the SOC is never attained if six nodes are perturbed. Non-local triggering of avalanches disturbs the long-range correlations necessary to the SOC state.

3.3. DRIVING MECHANISM

Georgoulis and Vlahos (1996, 1998) have designed a series of models where the field increments δB are extracted from a probability distribution having the form of a declining power-law: $p(\delta B) \sim \delta B^{-\alpha}$. They show that the usual power law indices α_E, α_P and α_T vary linearly with the index α of the above probability distribution, thus offering an attractive mechanism to tune (or induce temporal variability in) the logarithmic slopes of the frequency distributions.

Norman *et al.* (2001) have considered the effects of a non-stationary driving mechanism, by modulating the uniform driver of the basic model by a random walk function $\rho(t)$: $\delta B \in \rho(t) \times [\sigma_1, \sigma_2]$. The resulting statistical distributions of δB are characterized by extended tails (see their Figure 1), and lead to somewhat steeper frequency distributions of avalanche size parameters than in the uniform-driving case. Norman *et al.* also demonstrate that the average flaring rate in their models with non-uniform driving scales with the average energy input rate as a remarkably tight power law with index $\simeq 1.6$ (see their Figure 3).

The use of a non-stationary driver by Norman *et al.* (2001) was motivated by the analysis of Wheatland (2000b), suggesting that the power-law tail of the observed waiting time distribution could be understood in terms of a piecewise-constant Poisson process. The WTDs obtained by Norman *et al.* are indeed characterized by well-defined power-law tails at large waiting times, with the power-law index in reasonable agreement with observational inferences, as shown on Figure 8.

What happens if the weak driving condition $|\delta B|/\langle B\rangle \ll 1$ is violated? Small increments are better at bringing a large portion of the lattice close to the stability threshold, without exceeding it. Lattice-spanning avalanches can only materialize if such large clusters of marginally stable nodes have the opportunity to build up, something that becomes increasingly difficult as $\langle \delta B\rangle$ becomes comparable to $\langle B\rangle$. On the other hand, increasing $\langle \delta B\rangle$ also demands an increase in the frequency of boundary-discharging avalanches, if a stationary state is to be maintained. As a result of these two conflicting tendencies, strong driving ends up to favoring mid-size avalanches. As exemplified on Figure 9 for the peak energy P, the resulting frequency distributions of avalanche parameters do not show the well-defined power law so striking on Figure 6(B). The lattice is still stationary, still avalanching, and still dissipating energy, but it is no longer in a critical state. A similar situation materializes when the δB's are extracted from a distribution with zero mean (LHMB, Figure 5).

3.4. PROBABILISTIC MODELS

MacKinnon, Macpherson, and Vlahos (1996) have put forth a probabilistic model that reduces the stability condition and redistribution rule to the strict minimum. Their model is basically a 1-D forest-fire cellular automaton, mathematically akin to directed percolation (see Stauffer and Aharony, 1994, Chapter 6). Consider a 1D array of sites (nodes) that can be in either one of three possible states: loaded,

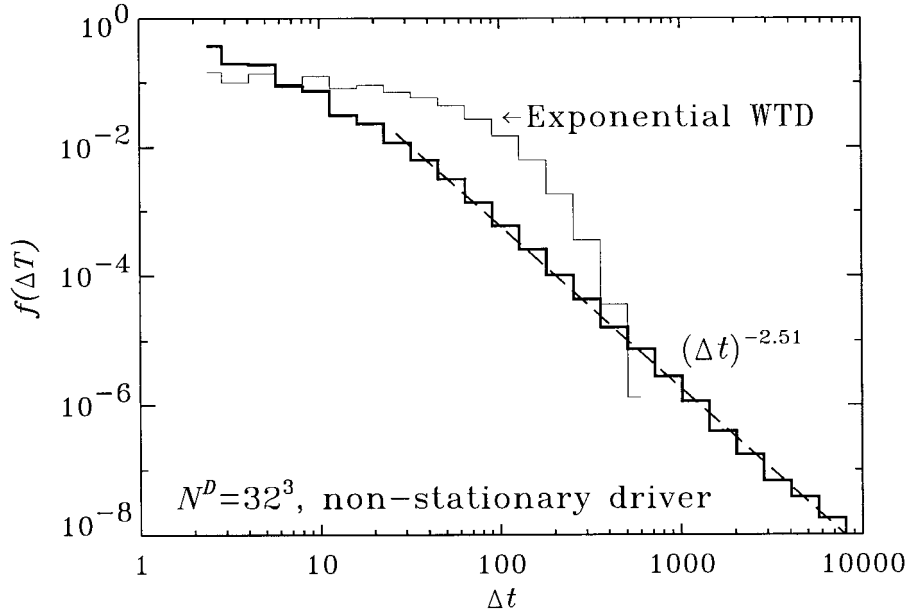

Figure 8. Waiting time distribution (*thick histogram*) for the non-stationary driving model of Norman *et al.* (2001). Beyond $t = 20$ (iteration units), the WTD is well fit by a power law with index 2.51 ± 0.16, in agreement within error bars with the observational value 2.4 ± 0.1 inferred by Boffeta *et al.* (1999), although somewhat larger than the value 2.16 ± 0.05 obtained by Wheatland (2000b). For comparison, the exponential WTD of the basic model with uniform driving is also shown.

flaring, or empty. The evolution rules are quite simple: *if* a loaded site has a nearest neighbor in a flaring state *then* flare at the next time step with probability p_1; *else*, flare spontaneously with probability p_0 ($\ll p_1$). A loaded site can flare only once, after which it remains empty[14].

The probability distribution of event size, defined as the number of sites undergoing flaring, is readily computed by considering the various ways in which events of size N can unfold, as shown on Figure 10. For example, there are two distinct ways to produce an event of size $N = 2$, each with probability $p_0 p_1 (1 - p_1)^2$: first, a site must be spontaneously activated (probability p_0); only one of the two neighbors must subsequently flare [probability $p_1(1 - p_1)$], but then its neighbor must fail to flare at the subsequent iteration [probability $(1 - p_1)$]. It follows that the probability of producing an event of size N is

$$p(N) = N p_0 p_1^{N-1} (1 - p_1)^2 \, . \tag{18}$$

Assume now that the flaring probability p_1 is a uniformly distributed random variable $p_1 \in [0, 1]$. Integrating Equation (18) over p_1 then leads to a frequency

[14]In the classical forest-fire model of Drossel and Schwabl (1992), an empty site can 'grow a tree' (reloading) with probability p_2; a SOC state is attained in the double limit $p_2 \ll 1$ and $p_0 \ll p_2$. (Jensen, 1998, Section 4.5; Sinha-Ray and Jensen, 2000).

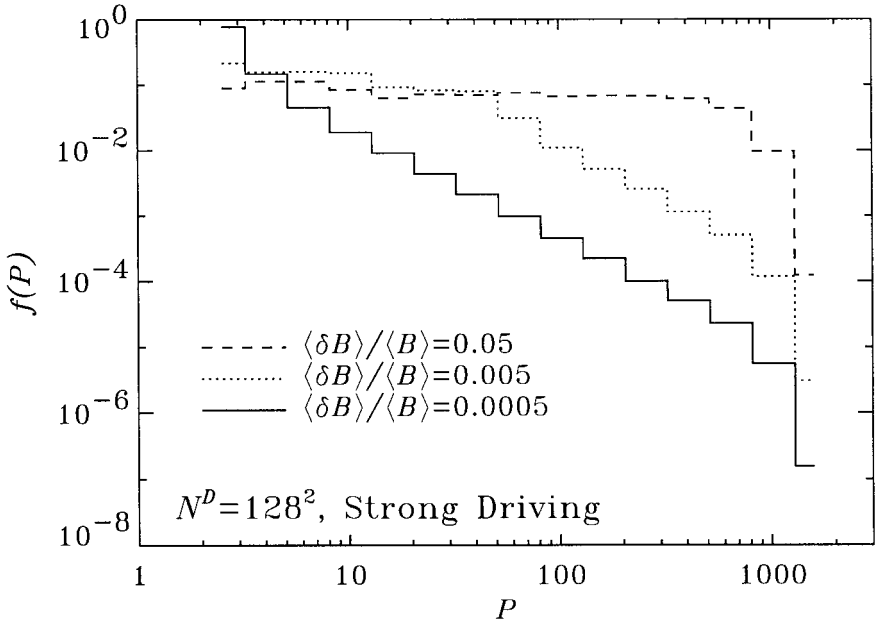

Figure 9. Frequency distribution of peak avalanche energy in $N^D = 128^2$, $Z_c = 5$ models with moderate to strong driving, as measured by $\langle\delta B\rangle/\langle B\rangle$ (cf., Section 2.4). Models with smaller values for this quantity yield $f(P)$ distributions statistically indistinguishable from the $\langle\delta B\rangle/\langle B\rangle = 0.0005$ model. Note that the latter has $\langle\delta B\rangle/Z_c = 0.68$, $\max(\Delta B)/Z_c = 2$, yet reached a *bona fide* SOC state.

distribution of event size: $f(N) \simeq 2/N^2$ (for $N \gg 1$). A power law thus results naturally from this simple interaction process. Branching theory suggests $\alpha_E \simeq 1.5$ for $D > 1$ (Litvinenko, 1998), while the 3D simulations of Macpherson and MacKinnon (1999) yield α_E in the range 1.76–2.87, depending on the assumed value of p_1, and whether and how fast empty sites are allowed to 'reload'. Note that this model is critical, but does not self-organize itself to criticality. Insight gained from studies of the forest fire model suggests that true SOC behavior might materialize upon introducing a 'reloading' probability p_2 such that $p_0 \ll p_2 \ll 1$, with $p_1 \lesssim 1$.

3.5. Lattice structure

To the best of our knowledge all work to date on the curvature-triggered model has been carried out on regular square ($D = 2$) or cubic ($D = 3$) lattices. Although these lattices are computationally convenient, such extreme regularity is hard to reconcile with Parker's picture of a complexly tangled magnetic field. Given what is known from percolation theory and lattice gas models, the global behavior on a triangular lattice (for example) is likely to be described by numerically distinct

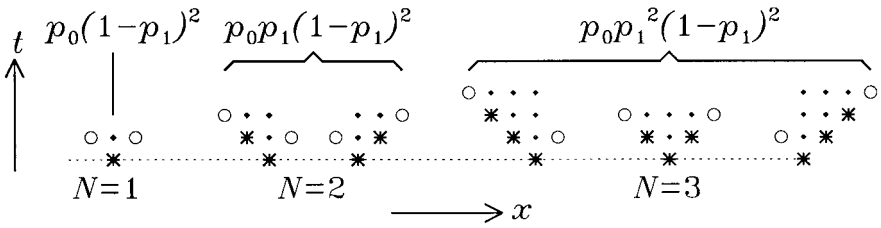

Figure 10. Probability $p(N)$ of observing an event of size N in the 1D cellular automaton model of MacKinnon, Macpherson, and Vlahos (1996). The probabilities of spontaneous and induced flaring are p_0 and p_1, respectively. The flaring sites are the $*$'s, and the loaded sites having failed to flare (probability $1 - p_1$) the $\circ$'s. Time runs upward, and sites having flares once already ($\cdot$) remain empty at all subsequent steps.

power-law indices. Clearly, more work is needed in exploring the consequences of alternate lattice geometries and connectivities.

4. Physical Interpretation

The success of SOC models at reproducing many statistical properties of solar flares has motivated a large body of work aimed at clarifying their underlying physical basis. We now turn to this important issue.

4.1. WHAT IS $B_{\mathbf{k}}$ ANYWAY?

The most straightforward physical association of the nodal field $B_{\mathbf{k}}$ is to the magnetic field $\mathbf{B}$, in which case Equation (3) for lattice energy and Equation (6) for nodal energy release make sense. However, in general this leads to $\nabla \cdot \mathbf{B} \neq 0$. LHMB point out that associating instead $B_{\mathbf{k}}$ with a vector potential $\mathbf{A}$ such that $\mathbf{B} = \nabla \times \mathbf{A}$ not only solves (trivially) the $\nabla \cdot \mathbf{B}$ problem[15], but also offers a plausible interpretation of the driving process. Adding an increment $\delta\mathbf{A}$ to the lattice amounts to locally twisting the magnetic field. Another attractive feature of this $B_{\mathbf{k}} \leftrightarrow \mathbf{A}$ *ansatz* is that it provides a physically meaningful interpretation for the instability threshold. As noted previously, Equation (4) has the form of a finite difference expression for the Laplacian operator, so that the threshold condition implies that 'reconnection' sets in once the local electric current ($\sim \nabla^2\mathbf{A}$ for a suitably selected gauge) exceeds a threshold value, which is physically appealing for reconnection-triggering plasma instabilities. However, $\sum B_{\mathbf{k}}^2$ is then no longer an obvious measure of lattice energy, which calls into question the whole idea of comparing model time series to flare observations.

[15]Another trivial solution to the $\nabla \cdot \mathbf{B} \neq 0$ problem is to consider a 2D lattice where $B_{\mathbf{k}}$ is the strength of a magnetic field oriented perpendicular to the lattice plane (e.g., Vassiliadis *et al.*, 1998). Evidently, this 'trick' is of limited applicability.

Interpreting the threshold and redistribution rule in term of anomalous diffusion (e.g., Isliker *et al.*, 1998; also Section 4.2 below), Isliker, Anastasiadis, and Vlahos (2000, 2001) also argue that $B_{\mathbf{k}}$ should be identified with a smooth vector potential, but sampled at *finite* spatial intervals corresponding to the characteristic diffusive length. They go on to argue that the redistribution rule can be interpreted in terms of current dissipation, and show that the frequency distributions of event sizes constructed using measures of current dissipation do not differ significantly from those arising from the traditional $B_{\mathbf{k}} \leftrightarrow \mathbf{B}$ interpretation (see Isliker, Anastasiadis, and Vlahos, 2000, Figure 3).

Alternately, one can associate $B_{\mathbf{k}}$ with a dynamically significant characteristic of a macroscopic physical object, such as a magnetic flux tube. Model B of Zirker and Cleveland (1993), as well as Chou's (1999) model, are of this type. Chou's $N^D = 50^2$ model associates $B_{\mathbf{k}}$ with the internal twist of flux tubes oriented perpendicular to the lattice plane (see also Chou, 2001). His stability criterion is defined in terms of the twist 'gradients' between *pairs* of neighboring nodes. Provided the redistribution conserves the twist (i.e., $B_{\mathbf{k}}$), the model behaves in manner analogous to the basic model of Section 2, and yields comparable power-law indices. In Zirker and Cleveland's (1993) Model B, only a small (20%) fraction of lattice node are occupied by flux tubes. Driving takes place by randomly moving flux tube footpoints to neighboring empty lattice nodes. In addition to twisting, the flux tubes can also wrap about one another ('braiding'). The braiding-related events lead to a power-law tail in the frequency distribution of energy release, but the power law index is found to be rather sensitively dependent on some model parameters.

Longcope and Noonan (2000) have constructed a $N^D = 30^2$ model where the dynamical elements are currents flowing along separatrix surfaces. The separatrix currents are driven by shearing in the lattice plane, and the threshold and redistribution rules both involve these currents. Tuning of a parameter results in power-law distributions of event sizes, with indices once again close to the corresponding indices for the basic 2D model at comparable N. This avalanche model is critical, but again lacks self-organization.

4.2. THE CONTINUUM LIMIT

It was already noted (Section 2.2) that the stability criterion given by Equation (4) has the functional form of a second-order centered finite difference expression for the D-dimensional Laplacian operator. This analogy can be exploited to construct a PDE describing the avalanching process. We first do so using the slightly (but, as we shall soon see, significantly) different redistribution rule introduced in the original LH91 paper. The $D = 1$ scalar stability criterion and redistribution rule are:

$$\Delta B_i^n = B_i^n - \frac{1}{2} \sum B_{i\pm1}^n \,, \tag{19}$$

$$B_i^{n+1} = B_i^n - \tfrac{2}{3}\Delta B_i^n \ , \qquad B_{i\pm1}^{n+1} = B_{i\pm1}^n + \tfrac{1}{3}\Delta B_i^n \ , \tag{20}$$

where i and n are the spatial and temporal indices, respectively. Note that $\Delta B_i^{n+1} = 0$ immediately after the distribution, unlike the LHMB rule adopted in our basic model of Section 2. In a region where contiguous nodes are avalanching, each node is subjected to three distinct increment/decrement operations, as per Equation (20). If nodal updates are carried out synchronously, as done in the algorithm of Figure 2, then the field variable at node i is updated according to

$$B_i^{n+1} = B_i^n - \tfrac{2}{3}\Delta B_i^n + \tfrac{1}{3}\Delta B_{i+1}^n + \tfrac{1}{3}\Delta B_{i-1}^n \ . \tag{21}$$

Making judicious use of Equation (19), this can be rewritten as

$$B^{n+1} - B^n = -\tfrac{2}{3}[S][S]B^n \ , \tag{22}$$

where $B \equiv B_i$, and the elements of the matrix $[S]$ are given by

$$[S]_{i,j} = \delta_{i,j} - \tfrac{1}{2}\delta_{i,j+1} - \tfrac{1}{2}\delta_{i,j-1} \ , \tag{23}$$

where $\delta_{i,j}$ is the Kronecker delta (see Liu *et al.*, 2001). Clearly, $[S]$ has the form of a second-order centered finite difference stencil for $(-1/2)\partial^2/\partial x^2$. Equation (22) is thus equivalent to the spatial discretization of the fourth-order hyperdiffusion equation:

$$B_t = -\kappa B_{xxxx} \ , \tag{24}$$

with second-order centered differencing in space (grid spacing $\Delta x = 1$), forward differencing in time (time step $\Delta t = 1$), and with a hyperdiffusion coefficient $\kappa = 1/6$ (subscripts 'x' and 't' are used hereafter to indicate partial derivatives with respect to space and time).

Some authors (Galsgaard, 1996; Macpherson, personal communication) have reported being unable to reproduce the LH91 results using their original redistribution rule. Our own numerical model, based on the algorithm given on Figure 2, eventually diverges if the LH91 rule is used, suggesting some sort of numerical instability. A standard von Neumann stability analysis (e.g., Press *et al.*, 1992, Section 19.1) can be applied to Equation (24), and yields an amplification factor

$$p = 1 - \frac{2}{3}\frac{\Delta t}{\Delta x^4}(\cos k\Delta x - 1)^2, \tag{25}$$

where the perturbation wavenumber k is real and non-negative. For $\Delta x = 1$, $\Delta t = 1$, $\max|p| = \frac{5}{3} > 1$ (for k such that $\cos k = -1$). Therefore, numerical integration of the difference equations (20) is *unconditionally unstable*. If instead only a fraction $f\Delta B_i$ ($0 < f < 1$) is redistributed in Equations (20), then the hyperdiffusion coefficient in Equation (24) becomes $\kappa = f/6$. It is easy to show that if $f < 3/4$, $\max|p| < 1\,\forall k$. Numerical experiments readily confirm this stability analysis.

The derivation leading to Equation (22) does not carry through if the LHMB redistribution rule is used, but evidently that rule is equivalent to introducing a multiplying factor $Z_c/|\Delta B_i|$ (< 1, since nodes are avalanching) to the redistributed quantity, and thus also to the hyperdiffusion coefficient associated with the LH91 rule. Although f now varies from node to node, this still suggests enhanced numerical stability, and indeed the use of the LHMB rule is found (empirically) to lead to a numerically stable model[16].

Equation (24) holds only in avalanching regions, but it should be nonetheless clear that in the continuum limit of $\Delta x \to 0$ and $\Delta t \to 0$, the lattice model of LH91 can be expressed as a randomly driven fourth order hyper-diffusive system with anomalous diffusion coefficient:

$$B_t = -(\kappa(B_{xx})B_{xxx})_x + f(x,t) \tag{26}$$

(written now in conservative form), where f is a low frequency random forcing, and

$$\kappa(B_{xx}) = \begin{cases} 0 & \text{if } |B_{xx}| < Z_c, \\ \frac{1}{6} & \text{if } |B_{xx}| > Z_c. \end{cases} \tag{27}$$

This conclusion actually carries over to the basic lattice model of Section 2, which uses instead the redistribution rule of LHMB. This is readily verified upon computing the power spectrum density of B in the SOC state, which yields a slope of -4, precisely what one would expect from a randomly driven fourth order diffusive system (see Liu *et al.*, 2001).

The avalanche equation possesses self-similar and traveling-wave solutions, just as the Kuramoto–Sivashinsky (Chang, 1986), the Cahn-Hilliard (Elliott and French, 1987), and the thin-film (Boatto, Kadanoff, and Olla, 1993), equations. These related higher-order diffusion equations have received significant attention in the literature (Smyth and Hill, 1988). Consider, for example, the curvature triggered hyper-diffusion equation

$$B_t = -(|B_{xx}|^{\nu} B_{xxx})_x \ . \tag{28}$$

This avalanche equation admits a self-similar solution of the form

$$B(x,t) = B_0\, t^{-\beta}\, b(xt^{-\beta}) \ , \tag{29}$$

with $\beta = 1/(4+3\nu)$. In terms of the variable $\xi \sim xt^{-\beta}$, one immediately deduces the nonlinear governing ODE,

$$|b_{\xi\xi}|^{\nu} b_{\xi\xi\xi} = \beta\xi b \ , \tag{30}$$

[16]The derivation of Equation (22) and subsequent stability analysis are pre-empted on synchronous update of all avalanching nodes. H. Isliker (personal communication) has indicated to us that a stable model based on the LH91 redistribution rule can be constructed by forsaking strict synchronicity in nodal updating.

for $b(\xi)$ an even function about $\xi = 0$, whose form is set by the adopted value of ν. The linear case ($\nu = 0$) admits solutions in terms of generalized hypergeometric functions. The avalanche front moves according to the power-law, $y \sim t^{1/4}$, as dictated by the form of the self-similar variable. For the general non-linear situation ($\nu \neq 0$), the motion of the front is slightly retarded, since $y \sim t^{1/(4+3\nu)}$.

We note finally that avalanching behavior is not restricted to fourth-order diffusion equations. Lu (1995b) has studied numerically the behavior of the second-order 1D avalanche equation

$$B_t = (\kappa(B_x)B_x)_x + f(x) \ , \tag{31}$$

with steady driving and $\kappa(B_x)$ described by a time-dependent threshold equation. He has shown that this system does produce self-similar energy dissipation via avalanches with sizes distributed as power laws. In the continuum limit as with the lattice model, a self-stabilizing threshold instability causing local transport emerges as the key ingredient. The exact form of the diffusion coefficient ($\equiv$ stability condition) and diffusion operator ($\equiv$ redistribution rule) is of secondary importance.

4.3. SOC-LIKE BEHAVIOR IN MHD TURBULENCE

It has now been amply demonstrated that energy dissipation in MHD turbulence occurs in a manner that is strongly intermittent, both spatially and temporally (e.g., Longcope and Sudan, 1994; Einaudi *et al.*, 1996; Galsgaard and Nordlund, 1996; Dmitruk and Gómez, 1997; Galtier and Pouquet, 1998; Georgoulis, Velli, and Einaudi, 1998; Einaudi and Velli, 1999; Galtier, 1999, and references therein). Such simulations are often characterized by a separation of timescales between driving and dissipation, and analysis of the time series of global energy dissipation yields flare-like time series, with the size distribution of dissipative events taking the form of a more or less well-defined power law. These features are attractively SOC-like. Yet, recall that the defining feature of SOC is interaction-dominated threshold dynamics. Can the large dissipative events measured in MHD simulations be interpreted as the superposition of numerous smaller events *triggering one another*? Or, do the observed power-law distributions of event sizes simply reflect the 'natural' size spectrum of the current sheets, each building up and dissipating *independently*? Expressed differently, does MHD turbulence exhibit avalanching behavior, or just self-similarity in the buildup of dissipative structures? Such questions are at the heart of the SOC interpretation of MHD turbulence, and at this writing remain unanswered.

5. Concluding Comments

We close this tutorial/review paper with a selective, brief overview of remaining problems or challenges, as well as areas where, in our opinion, the full potential of avalanche models has not yet been exhausted.

5.1. Flares and coronal heating

Perhaps the most impressive success of the avalanche model for solar flares remains its ability to reproduce the power-law form of the inferred frequency distributions of flare parameters, and to yield logarithmic slopes that are in good agreement with observations. The basic model of Section 2 does so without any fine tuning of model parameters, and is robust with respect to most aspects of the model's formulation.

This good agreement does not augur well for coronal heating, however. Recall from Section 1.2 that Parker's nanoflare conjecture requires $\alpha_E > 2$, which is *not* supported by most avalanche models, which (in principle) yield the true frequency distribution of energy release size. The situation is troublesome, because it is not easy to modify the model to get $\alpha_E > 2$ and, if one succeeds, the agreement with flare observations might well vanish. To the best of our knowledge the only extant construct that manages to satisfy both constraints is the 'double power law' hybrid model put forth by Georgoulis and Vlahos (1996, 1998; also Section 3.2 herein). This works provided that the steeper power law still lies below current detection thresholds. The recent determinations of flares energies down to about 10^{24} erg (Aschwanden *et al.*, 2000b), with no sign of a significant steepening of the frequency distribution, renders this position increasingly untenable (but see Mercier and Trottet, 1997).

5.2. Flare prediction

The conjectured SOC state of the solar corona has some disturbing consequences for flare forecasting, a topic of great interest among space weather aficionados. In the SOC state, whether large or small, an avalanche begins with one node exceeding the stability threshold following an external perturbation. It is certainly the case that 'kicking' a lattice already in its SOC state with a large perturbation (mimicking magnetic flux emergence in an existing active region, say), is very likely to trigger a large avalanche. On the other hand, an equally large avalanche can be triggered by a very small, unobservable perturbation. The former avalanche/flare can perhaps be predicted by identifying suitable precursors of flux emergence; the latter typifies a class of large flares that is quite simply unpredictable. This lack of predictability can be ascertained quantitatively by computing the Hurst exponent (H) of the model's energy release time series (e.g., Hastings and Sugihara, 1993, Chapter 4; Steeb, 1999, Section 2.4) compressed to the driving timescale (i.e., avalanches are

replaced by their peak energy release at a single iteration; see LHMB, Figure 2). This results in $H \simeq 0.5$, implying no 'memory', and thus no predictability[17].

5.3. THE FRACTAL NATURE OF AVALANCHES

If solar flares are indeed the manifestation of reconnection avalanches in a tangled coronal magnetic field, then the analysis of flare observations must come to grips with the fractal nature of avalanches in the SOC state. Specifically, the relationship between the volumetric energy release (E) and (observed) projected area (A) of X-ray or EUV emission is neither $E \sim A$ (cylinder model with constant column depth; see also Mitra-Kraev and Benz, 2001), nor $E \sim A^{3/2}$ (loop model; cf., Aschwanden *et al.*, 2000b, Section 2.1). The situation is further complicated by the fact that the avalanche area (Figure 5(D)), which would presumably be the structure 'seen' (in projection) by observations with exposure times comparable to the avalanche lifetime, has a fractal index significantly different from that of the avalanche at its peak (Figure 5(B)), which is presumably what observations at high temporal resolution would 'see'. Some of these issues are explored in McIntosh *et al.* (2001), where it is argued that such observations offer a unique observational test of SOC models for solar flares (see also the animations on the accompanying CD).

5.4. THE SOLAR CORONA AND SELF-ORGANIZED CRITICALITY

Is the solar coronal magnetic field in a self-organized critical state? We concur with Lu (1995a) that the coronal field does meet the requirements for the appearance of SOC: self-stabilizing local threshold instability; open boundaries; and separation of timescales between driving and avalanching. Moreover, Parker's picture of a complexly tangled coronal magnetic field driven to episodic localized reconnection by slow, random photospheric footpoint motions provides a sound physical underpinning to what is otherwise a model containing embarrassingly little of the MHD physics relied upon by the overwhelming majority of extant flare models. Naturally, this does not necessarily imply that the solar corona *is* in fact in a SOC state. We do hope at least to have convinced our readers that if it is, the consequences for our understanding of flares and coronal heating are many and far reaching.

[17] Unpublished Hurst exponent calculations carried out by J. Norman during his summer 2000 stay at HAO as an undergraduate research intern. Note, however, that Lepreti, Carbone, and Veltri (2001) have suggested that the solar flare WTD distribution is best fit with a Levy distribution, which would imply some level of memory (see Sornette, 2000, Section 4.1.4). The memory question clearly warrants further investigation.

Acknowledgements

This paper is a by-product of the activities of the SOC working group at HAO/NCAR, which for a summer counted within its ranks James Norman (University of Newcastle upon Tyne/U.K.), whose valuable contributions we wish to acknowledge. We also benefited from discussions and/or e-mail exchanges with Ed Lu, Klaus Galsgaard, Annick Pouquet, and Heinz Isliker. We also wish to thank Sarah Gibson and an anonymous referee for a careful reading of the paper. SWM was supported up to January 2001 through the Advanced Study Program at NCAR, and since then by an ESA External Fellowship at NASA/GSFC. HLL is partly supported through NASA grant S-97239-E to NCAR. The National Center for Atmospheric Research is sponsored by the National Science Foundation.

References

Aschwanden, M. J., Dennis, B. R., and Benz, A. O.: 1998, *Astrophys. J.* **497**, 972.
Aschwanden, M. J., Nightingale, R. W., Tarbell, T. D., and Wolfson, C. J.: 2000a, *Astrophys. J.* **535**, 1027.
Aschwanden, M. J., Tarbell, T. D., Nightingale, R. W., Schrijver, C. J., Title, A., Kankelborg, C. C., Martens, P., and Warren, H. P.: 2000b, *Astrophys. J.* **535**, 1047.
Audard, M., Güdel, M., Drake, J. J., and Kashyap, V. L.: 2000, *Astrophys. J.* **541**, 396.
Bak, P.: 1996, *How Nature Works*, Springer/Copernicus, New York.
Bak, P., Tang, C., and Wiesenfeld, K.: 1987, *Phys. Rev. Lett.* **59**, 381 (BTW).
Bak, P., Tang, C., and Wiesenfeld, K.: 1988, *Phys. Rev.* **A38**, 384.
Boatta, S., Kadanoff, L. P., and Olla, P.: 1993, *Phys. Rev.* **E48**, 4423.
Boffeta, G., Carbone, V., Veltri, P., and Vulpiani, A. 1999, *Phys. Rev. Lett.* **83**, 4662.
Bromund, K. R., McTiernan, J. M., and Kane, S. R.: 1995, *Astrophys. J.* **455**, 733.
Brown, J. C., McArthur, G. K., Barrett, R. K., McIntosh, S. W., and Emslie, A. G.: 1998, *Solar Phys.* **179**, 379.
Carrington, R. C.: 1860, *Monthly Notices Roy. Astron. Soc.* **20**, 13.
Chang, H.-C.: 1986, *Phys. Fluids* **29**, 3142.
Chessa, A., Stanley, H. E., Vespignani, A., and Zapperi, S.: 1999, *Phys. Rev.* **E59**, R12.
Chou, Y.-P.: 1999, *Astrophys. J.* **527**, 958.
Chou, Y.-P.: 2001, *Solar Phys.* **199**, 345.
Crosby, N. B., Aschwanden, M. J., and Dennis, B. R.: 1993, *Solar Phys.* **143**, 275.
Crosby, N. B., Vilmer, N., Lund, N., and Sunyaev, R.: 1998, *Astron. Astrophys.* **334**, 299.
Datlowe, D. W., Elcan, M. J., and Hudson, H. S.: 1974, *Solar Phys.* **39**, 155.
Dennis, B. R.: 1985, *Solar Phys.* **100**, 465.
Dmitruk, P. and Gómez, D. O.: 1997, *Astrophys. J.* **484**, L83.
Drake, J. F.: 1971, *Solar Phys.* **16**, 152.
Drossel, B. and Schwabl, F.: 1992, *Phys. Rev. Lett.* **69**, 1629.
Duran, J.: 2000, *Sands, Powders, and Grains*, Springer-Verlag, Berlin.
Edney, S. D., Robinson, P. A., and Chisholm, D.: 1998, *Phys. Rev.* **E58**, 5395.
Einaudi, G. and Velli, M.: 1999, *Phys. Plasmas* **6**, 414.
Einaudi, G., Velli, M., Politano, H., and Pouquet, A.: 1996, *Astrophys. J.* **457**, L113.
Elliott, C. M. and French, D. A.: 1987, *IMA J. Appl. Math.* **38**, 97.
Galsgaard, K.: 1996, *Astron. Astrophys.* **315**, 312.

Galsgaard, K., and Nordlund, Å.: 1996, *J. Geophys. Res.* **101**, 13445.
Galtier, S.: 1999, *Astrophys. J.* **521**, 483.
Galtier, S. and Pouquet, A.: 1998, *Solar Phys.* **179**, 141.
Georgoulis, M. K. and Vlahos, L.: 1996, *Astrophys. J.* **469**, L135.
Georgoulis, M. K. and Vlahos, L.: 1998, *Astron. Astrophys.* **336**, 721.
Georgoulis, M. K., Velli, M., and Einaudi, G.: 1998, *Astrophys. J.* **497**, 957.
Georgoulis, M. K., Vilmer, N., and Crosby, N. B.: 2001, *Astron. Astrophys.* **367**, 326.
Hastings, H. M. and Sugihara, G.: 1993, *Fractals. A User's Guide for the Natural Sciences*, Oxford University Press, Oxford.
Hoyt, D. V. and Schatten, K. H.: 1997, *The Role of the Sun in Climate Change*, Oxford University Press, Oxford.
Isliker, H., Anastasiadis, A., and Vlahos, L.: 2000, *Astron. Astrophys.* **363**, 1134.
Isliker, H., Anastasiadis, A., and Vlahos, L.: 2001, *Astron. Astrophys.* **377**, 1068.
Isliker, H., Anastasiadis, A., Vassiliadis, D., and Vlahos, L.: 1998, *Astron. Astrophys.* **335**, 1085.
Jensen, H. J.: 1998, *Self-Organized Criticality*, Cambridge University Press, Cambridge.
Kadanoff, L. P., Nagel, S. R., Wu, L., and Zhou, S.: 1989, *Phys. Rev* **A39**, 6524.
Krucker, S. and Benz, A. O.: 1998, *Astrophys. J.* **501**, L213.
Krucker, S. and Benz, A. O.: 2000, *Solar Phys.* **191**, 341.
Kulsrud, R. M.: 1998, *Phys. Plasmas* **5**, 1599.
Lee, T. T., Petrosian, V., and McTiernan, J. M.: 1993, *Astrophys. J.* **412**, 401.
Lepreti, F., Carbone, V., and Veltri, P.: 2001, *Astrophys. J.* **555**, L133.
Litvinenko, Y. E.: 1996, *Solar Phys.* **167**, 321.
Litvinenko, Y. E.: 1998, *Astron. Astrophys.* **339**, L57.
Liu, H.-L., Charbonneau, P., Bogdan, T. J., Pouquet, A., and McIntosh, S. W.: 2001, *Phys Rev E* (in preparation).
Longcope, D. W. and Noonan, E. J.: 2000, *Astrophys. J.* **542**, 1088.
Longcope, D. W. and Sudan, R. N.: 1994, *Astrophys. J.* **437**, 491.
Lu, E. T.: 1995a, *Astrophys. J.* **446**, L109.
Lu, E. T.: 1995b, *Phys. Rev. Lett.* **74**, 2511.
Lu, E. T.: 1995c, *Astrophys. J.* **447**, 416.
Lu, E. T. and Hamilton, R. J.: 1991, *Astrophys. J.* **380**, L89 (LH91).
Lu, E. T., Hamilton, R. J., McTiernan, J. M., and Bromund, K. R.: 1993, *Astrophys. J.* **412**, 841 (LHMB).
Luke, Y. L.: 1962, *Integrals of Bessel Functions*, McGraw-Hill, New York.
MacKinnon, A. L. and Macpherson, K. P.: 1997, *Astron. Astrophys.* **326**, 1228.
MacKinnon, A. L., Macpherson, K. P., and Vlahos, L.: 1996, *Astron. Astrophys.* **310**, L9.
Macpherson, K. P. and MacKinnon, A. L.: 1999, *Astron. Astrophys.* **350**, 1040.
McIntosh, S. W., Charbonneau, P., Bogdan, T. J., Liu, H.-L., and Norman, J. P.: 2001, *Phys. Rev. E.* (submitted).
Mercier, C. and Trottet, G.: 1997, *Astrophys. J.* **474**, L65.
Mikić, Z., Schnack, D. D., and Van Hoven, G.: 1989, *Astrophys. J.* **338**, 1148.
Mitra-Kraev, U. and Benz, A. O.: 2001 *Astron. Astrophys.* **373**, 318.
Nagel, S. R.: 1992, *Rev. Mod. Phys.* **64**, 321.
Newman, M. E. J. and Sneppen, K.: 1996, *Phys. Rev.* **E54**, 6226.
Norman, J. P., Charbonneau, P., McIntosh, S. W., and Liu, H.-L.: 2001, *Astrophys. J.* **557**, 891.
Osten, R. A. and Brown, A.: 1999, *Astrophys. J.* **515**, 746.
Parker, E. N.: 1983, *Astrophys. J.* **264**, 642.
Parker, E. N.: 1988, *Astrophys. J.* **330**, 474.
Parker, E. N.: 1994, *Spontaneous current sheets in magnetic fields*, Oxford University Press, New York.
Parnell, C. E. and Jupp, P. E.: 2000, *Astrophys. J.* **529**, 554.

Porter, J. G., Moore, R. L., Reichmann, E. J., Engvold, O., and Harvey, K. L.: 1987, *Astrophys. J.* **323**, 380.
Press, W. H., Teukolsky, S. A., Vetterling, W. T., and Flannery, B. P.: 1992, *Numerical Recipes*, 2nd ed., Cambridge University Press, Cambridge.
Priest, E. and Forbes, T.: 2000, *Magnetic Reconnection*, Cambridge University Press, Cambridge.
Robinson, P. A.: 1994, *Phys. Rev.* **E49**, 1984.
Rosner, R. and Vaiana, G.: 1978, *Astrophys. J.* **222**, 1104.
Shakhovskaya, N. I.: 1989, *Solar Phys.* **121**, 375.
Shimizu, T.: 1995, *Publ. Astron. Soc. Japan* **47**, 251.
Shimojo, M. and Shibata, K.: 1999, *Astrophys. J.* **516**, 934.
Sinha-Ray, P. and Jensen, H. J.: 2000, *Phys. Rev.* **E62**, 3215.
Smyth, N. F. and Hill, J. M.: 1988, *IMA J. Appl. Math.* **40**, 73.
Sornette, D.: 2000, *Critical Phenomena in Natural Sciences*, Springer-Verlag, New York.
Steeb, W.-H.: 1999, *The Nonlinear Workbook*, World Scientific, Singapore.
Stauffer, D. and Aharony, A.: 1994, *Introduction to Percolation Theory*, 2nd ed., Taylor and Francis, London.
Sturrock, P. A., Dixon, W. W., Klimchuk, J. A., and Antiochos, S. K.: 1990, *Astrophys. J.* **356**, L31.
Turcotte, D. L.: 1999, *Rep. Prog. Phys.* **62**, 1377.
van Ballegooijen, A. A.: 1986, *Astrophys. J.* **311**, 1001.
Vassiliadis, D., Anastasiadis, A., Georgoulis, M., and Vlahos, L. 1998, *Astrophys. J.* **509**, L53.
Vlahos, L., Georgoulis, M., Kluiving, R., and Paschos, P.: 1995, *Astron. Astrophys.* **299**, 897.
Wheatland, M. S.: 1999, *Solar Phys.* **191**, 381.
Wheatland, M. S.: 2000a, *Astrophys. J.* **532**, 1209.
Wheatland, M. S.: 2000b, *Astrophys. J.* **536**, L109.
Wheatland, M. S. and Glukhov, S.: 1998, *Solar Phys.* **167**, 321.
Wheatland, M. S., Sturrock, P. A., and McTiernan, J. M.: 1998, *Astrophys. J.* **509**, 448.
Withbroe, G. L. and Noyes, R. W.: 1977, *Ann. Rev. Astron. Astrophys.* **15**, 363.
Zirker, J. B. and Cleveland, F. M.: 1993, *Solar Phys.* **145**, 119.